Original Paper

Temperature dependence of Er nanostructure on InP(001)

T. Mochizuki[1], S. Yagi[1]*, M. Kato[1], K. Soda[1], H. Namatame[2] and M. Taniguchi[2]

Material analysis station & Advanced nano characterization center, National Institute for Material Science,

[1]*Department of Quantum Engineering, Graduate School of Engineering, Nagoya University, Furo-cho, Chikusa-ku,*
Nagoya 464-8603, Japan

[2]*Hiroshima Synchrotron Radiation Center, Hiroshima University,*
2-313 Kagamiyama, Higashi-hiroshima 739-0046, Japan

s-yagi@nucl.nagoya-u.ac.jp

The surface morphology, local structure and chemical states of Er nanostructure formed by Er deposition on the clean InP(001)-2×4 surface have been investigated by means of atomic force microscopy (AFM), extended and near edge X-ray absorption fine structures (EXAFS and NEXAFS). The nanodots are observed on the substrate by AFM. The size of these nanodots increases with substrate temperature. The EXAFS results show that ErP nanostructures are formed with a tetrahedral bond at substrate temperature T_s = 573 K and in the NaCl-structure at T_s = 673 and 773 K.

1. Introduction

Rare Earth (RE) compounds have been paid much attention as new functional materials because of their magnetic and electronic properties. Since Er pnictides have lattice constants similar to that of III-V semiconductors, they are regarded as candidate materials for high-speed magneto-electronic and magneto-optical devices [1]. Furthermore, an ErP nanostructure on InP (ErP/InP) shows a semimetal-semiconductor transition due to the quantum size effect [2]. However, ErP/InP can be grown by a low-pressure organometallic vapor phase epitaxy (OMVPE) method [3-5]. ErP/InP prepared by this method may be affected with impurities such as carbon and oxygen [4]. Thus, we have tried to fabricate the nanodots of ErP by Er deposition onto InP substrate under ultra high vacuum condition. In this study, we have revealed their surface morphology, local structure and chemical states by means of atomic force microscopy (AFM), extended X-ray absorption fine structure (EXAFS) and near edge X-ray absorption fine structure (NEXAFS), respectively.

2. Experimental

An undoped n-type InP(001) wafer was used as a substrate. A clean InP(001)-2×4 surface of the substrates was achieved by a sputtering (0.5 keV, 60 min) and annealing (587 K, 10 min) method after chemical etching with a solution of H_2SO_4:H_2O_2:H_2O = 4:1:1 and hydrogen termination with 50% NH_3F at room temperature. Samples of nanostructured Er on the InP(001) surface were fabricated by the Er deposition with an electron bombardment method at various substrate temperatures T_s =573, 673 and 773 K. Samples fabricated at T_s = 573, 673 and 773 K were described A, B and C. The base pressure was $3×10^{-8}$ Pa, and the pressure during Er deposition was kept below $5×10^{-7}$ Pa. The amount of the Er deposition was estimated as thickness in the unit of monolayer (ML) by use of a quarts microbalance calibrated by Rutherford backscattering spectroscopy (RBS) measurement at a Van de Graff accelerator AN-2500 in the Ion Beam Surface Analysis Laboratory at Nagoya University. Here, 1 ML is defined as $5.80×10^{14}$ atoms cm^{-2}. T_s and the amount of Er deposited for the samples A, B and C are listed in Table 1. While the sample A shows no low energy electron diffraction (LEED) pattern, the samples B and C show a diffuse 1×1 and a sharp 4×1 patterns, respectively.

Surface morphology was observed by an AFM (Veeco, NanoScope IIIa) with the tapping mode. Both EXAFS and NEXAFS measurements of Er L_3-edge at room tem

Journal of Surface Analysis Vol.14, No. 4 (2008) pp. 449-452

T. Mochizuki et al.   Temperature dependence of Er nanostructure on InP(001)

Table.1. Substrate temperature T_s and the amount of Er deposited for the samples A, B and C.

Sample	Substrate Temperature (K)	Amount of Er deposition (ML)
#A	573	35
#B	673	20
#C	773	~ 80

perature were carried out by a fluorescence yield detection at the X-ray Development and Demonstration (XDD) beam line of SSLS, Singapore Synchrotron Light Source in National University of Singapore [6].

3. Results and Discussion

The AFM images of the Er/InP samples A, B, and C are shown in the Fig. 1 (a), (b) and (c), respectively. For the sample A, many spherical nano-sized particles shown in the circle are formed on the InP surface. While, small spherical shaped nanoparticles shown in the circle and large shapeless nanoparticles indicated by the arrow are formed in the sample B. In the image of the sample C, nanoparticles are also observed on the surface. However, not shown here, many huge islands with several m in size appear in the wide range image. The size distributions in the range of 30 nm for the nanoparticles are presented in Fig. 1 (d), (e) and (f). Here, the nanoparticle size is defined by its height of the AFM image. The particle size with a standard deviation can be evaluated by the height value of the AFM analysis [7, 8]. The averaged particle size is 8.0±4.2 nm for the sample A, 8.7±3.6 nm for B and 9.1±5.8 nm for C. It is found that the particle size gradually increases with T_s.

The Fourier transform of the Er L_3-edge EXAFS spectra $k^3\chi(k)$ for samples A, B, and C as well as Er powder are shown in Fig. 2. The best-fitted parameters of bond lengths r and coordination numbers N with the bond assignments around Er are listed in Table 2. These EXAFS analyses were carried out with the code Rex2000 [9], and the Fourier transformation was performed in the range of 0.2–0.7 nm^{-1}. Since a peak "c" appears largely for the Er powder and peaks "a and b" are observed at the same position in the results of Ofuchi et al. [4], the peaks "a", "b" and "c" are assigned to the bond of Er-O, Er-P and Er-Er, respectively. The Er-P bond length increases from
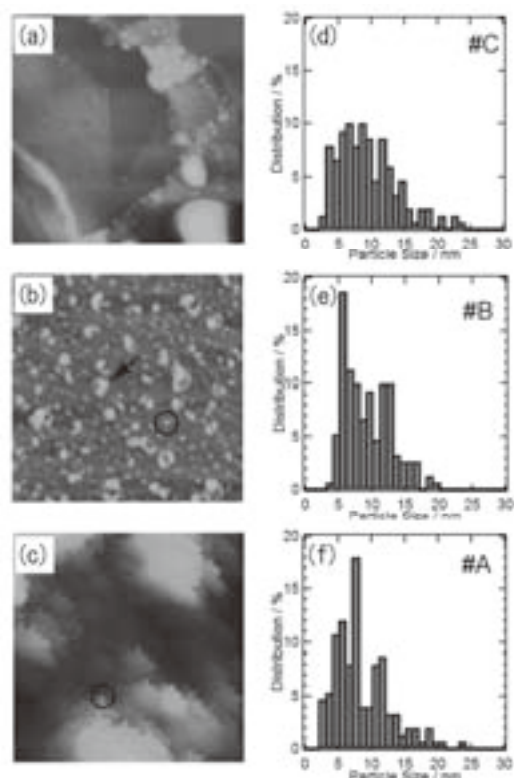

Fig.1. AFM images and particle size distribution of Er/InP samples A in the panels (a) and (d), B in (b) and (e), and C in (c) and (f) respectively. The size of the scanned area is 2×2 μm².
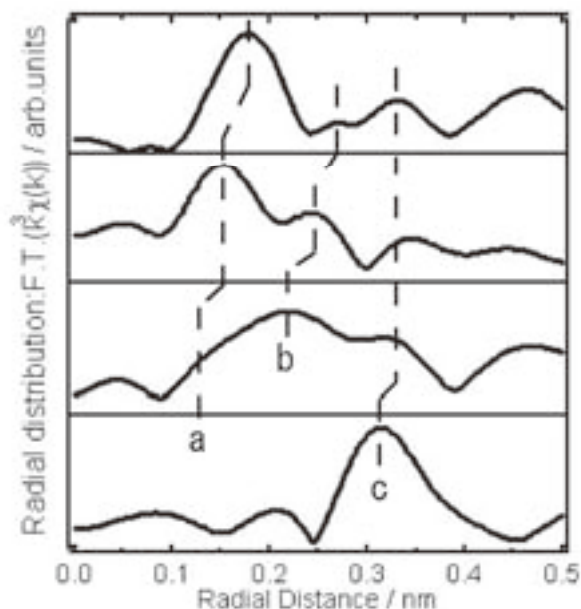

Fig.2. Fourier transform of Er L_3-edge EXAFS $k^3\chi(k)$ spectra of samples A, B, C and Er powder.

Table.2. Coordination numbers N and bond lengths r estimated from the Er L_3-edge EXAFS spectra of sample A, B, C and Er powder.

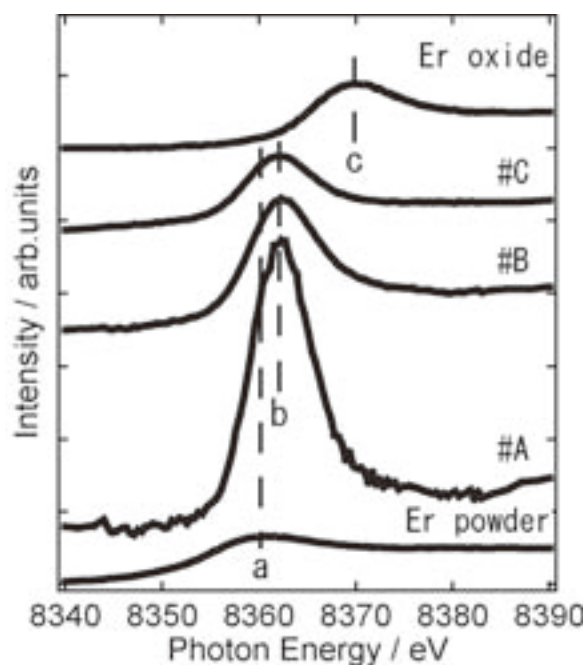| Sample	Bond	N	r (nm)
Er powder	Er-Er	2.8	0.354
#A	Er-Er	8.3	0.350
	Er-O	3.1	0.227
	Er-P	3.9	0.263
#B	Er-Er	4.0	0.353
	Er-O	6.0	0.225
	Er-P	4.2	0.283
#C	Er-Er	4.0	0.350
	Er-O	3.3	0.226
	Er-P	1.7	0.289
	Er-In	4.0	0.319

Fig.3. Er L_3-edge NEXAFS spectra of samples A, B and C. The spectra of Er powder and oxidized Er powder are also shown as reference.

0.267 nm for the sample A, which is equal to the sum of Er (0.157 nm) and P (0.110 nm) covalent radii in the tetrahedral structure, to 0.283 - 0.289 nm for the samples B and C. These values are close to 0.280 nm which is known as the Er-P bond length in the NaCl-structure [10]. However, the coordination number N_p of Er-P for the samples B and C are smaller than that of 6 in the NaCl-structure. It might be caused by the deficiency of P atoms because of its high vapor pressure at higher substrate temperature T_s. On the other hand, the obtained

Er-Er bond length of 0.350 – 0.354 nm and those of the Er-O of 0.225 – 0.227 nm do not change so much in all the samples: the Er-Er bonds are almost twice as long as the atomic radius of 0.176 nm [11], and the Er-O bond lengths are nearly the same as those reported so far, 0.219 – 0.223 nm, for the OMVPE-grown ErP/InP and Er_2O_3 powder [4]. As T_s increases from 573 to 673 K, the coordination number N_{Er} of Er-Er decreases, while that N_O of Er-O increases. Further increase in T_s from 673 to 773 K leads to the reduction in N_P and N_O as well as the appearance of a coordination of Er-In. These findings may suggest the formation of ErP in all the samples. The obtained coordination number N_{Er} for Er powder is small due to the self-absorption of Er.

Fig. 3 shows the Er L_3-edge NEXAFS spectra of the samples A, B and C in comparison with those of metallic and oxide Er powders. These spectra are normalized by the edge-jump, which means the intensity difference between the photon energies of 8340 and 8390 eV. Only a small peak "a" appears in the spectrum for Er powder, while large peaks "b" and small shoulders "a" are observed in samples A, B and C. For Er oxide, only higher-energy peak "c" is obtained. Therefore, the peaks "a", "b" and "c" are assigned to the bond of Er-Er, Er-P and Er-O, respectively. For the samples A, B and C, shoulder structures of Er-Er bond are seen, and the intensity of the peak "b" decreases at higher substrate temperature T_s. These agree with the results of EXAFS, *i.e.* appearance of Er-Er bond and deficiency of P atoms. On the other hand, the degree of oxidation is not so large for the Er/InP samples, compared to the Er oxide. We assume that the formation of the Er-O bond, *i.e.* the oxidation of Er, is due to the *ex-situ* EXAFS and NEXAFS measurements and is not caused at the fabrication. It is necessary to measure the *in-situ* EXAFS and NEXAFS spectra in future.

4. Conclusion

We have investigated the surface morphology, local structure and chemical states of Er nanostructures on the InP(001) substrate fabricated by the vacuum deposition method at various substrate temperatures T_s by the AFM, Er L_3-edge EXAFS and NEXAFS techniques. The obtained results show that ErP nanostructures are formed with a tetrahedral structure at T_s = 573 K and in the NaCl-structure at T_s= 673 and 773 K. Since the affection

of oxygen is observed in *ex-situ* measurements, it is important to measure with *in-situ* system.

6. References

[1] N. Jourdan, H. Yamaguchi, Y. Horikoshi, Jpn. J. Appl. Phys. **32,** L1784 (1993).

[2] T. Akane, S. Jinno, Y. Yang, T. Kuno, T. Hirata, Y. Isogai, N. Watanabe, Y. Fujiwara, A. Nakamura, Y. Takeda, Appl. Surf. Sci. **216**, 537 (2003).

[3] H. Ofuchi, D. Kawamura, N. Matsubara, M. Tabuchi, Y. Fujiwara, Y. Takeda, Microelectronic Eng. **43-44**, 745 (1998).

[4] H. Ofuchi, T. Akane, S. Jinno, T. Kuno, T. Hirata, M. Tabuchi, Y. Fujiwara, Y.Takeda, A. Nakamura, Mater. Sci. in Semicon. Process. **6**, 469 (2003).

[5] L. Bolotov, T. Tsuchiya, A. Nakamura, T. Ito, Y. Fujisawa, Y. Takeda, Phys. Rev. B **59**, 12236 (1999).

[6] H.O. Moser, B.D.F. Casse, E.P. Chew, M. Cholewa, C.Z. Diao, S.X.D. Ding, J.R. Konf, Z.W. Li, Miao Hua, M.L. Ng, B.T. Saw, Sharain bin Mahmood, S.V. Vidyaraj, O. Wilhelmi, J. Wong, P. Yang, X.J. Yu, The 5th Asian Synchrotron Radiation Forum, March 16-17 (2004).

[7] S. Yagi, H. Sumida, K. Miura, T. Nomoto, K. Soda, H. Namatame, M. Taniguchi, e-J. Surf. Sci. Nanotech. **4,** 258 (2006).

[8] T. Ashida, K. Miura, T. Nomoto, S. Yagi, H. Sumida, G. Kutluk, K. Soda, H. Namatame, M. Taniguchi, Surf. Sci. **601**, 3898 (2007).

[9] Rigaku EXAFS Analysis Software, REX2000, Cat. No. 2612S311/312/321/322, Rigaku Co., (2000).

[10] A. Guivarc'h, J. Caulet, A. Le Corre, Electron. Lett. **25**, 1050 (1989).

[11] W.B. Pearson, Crystal Chimistry and Physics of Metals and Alloys, Wiley, (1972).